Interannual Variability in the Thermodynamics of Subduction over the North Atlantic

ALISON J. MCLAREN AND RICHARD G. WILLIAMS

Oceanography Laboratories, Department of Earth Sciences, University of Liverpool, Liverpool, United Kingdom

(Manuscript received 31 October 2000, in final form 16 April 2001)

ABSTRACT

Subduction requires a buoyancy input into the mixed layer, which over the gyre scale can either be achieved by an atmospheric input or a wind-induced Ekman redistribution of buoyancy. The buoyancy budget for subduction is diagnosed over the North Atlantic using monthly fields from 1950 to 1992. The climatological-mean budget suggests that subduction over the subtropical gyre occurs through an Ekman redistribution of buoyancy from the Tropics, rather than a surface buoyancy flux from the atmosphere. In contrast, interannual variations in subduction are controlled by the variations in the surface buoyancy flux, which are generally greater than the variations in the Ekman redistribution of buoyancy. However, over the Tropics and southern part of the subtropical gyre, there is a partial cancellation in the opposing contributions from the surface and Ekman buoyancy fluxes, which acts to reduce the interannual variations in subduction.

1. Introduction

Over the North Atlantic, there are marked interannual variations in the atmosphere and ocean, as revealed in large-scale changes in sea surface temperature and sea level pressure (Bjerknes 1964; Kushnir 1994), diagnosed surface heat fluxes (Cayan 1992a), and patterns of deep convection (Dickson et al. 1996). Cayan (1992b) argued that atmospheric anomalies drive changes in the ocean since the tendency in sea surface temperature anomalies in winter correlate with latent and sensible heat flux anomalies. However, the mechanisms by which the ocean subsequently responds to interannual changes in atmospheric forcing are unclear. Here we focus on how the subduction process is altered through changes in atmospheric forcing.

Oceanic subduction determines the heat content and water-mass structure of the upper ocean. Fluid is transferred or subducted from the mixed layer into the upper thermocline through a combination of the circulation and buoyancy forcing. The subducted fluid is then insulated from the atmosphere until the fluid is reentrained back into the mixed layer in another location. Consequently, the subduction process provides a memory in the coupled atmosphere–ocean system.

A climatological view of subduction over the North Atlantic has been provided by Marshall et al. (1993, henceforth MNW). The annual subduction rate is evaluated in terms of the vertical and lateral volume flux passing through a control surface, defined by the base of the mixed layer at the end of winter (Fig. 1a). This control surface deepens poleward from 100 m in the middle of the subtropical gyre to 500 m or more in the subpolar gyre. Wind forcing induces downwelling of surface fluid over the subtropical gyre and upwelling over the subpolar gyre, which reaches magnitudes of typically 25 m yr^{-1} at the base of the winter mixed layer. Fluid is also transferred laterally from the winter mixed layer into the stratified thermocline. The resulting subduction rate into the main thermocline reaches between 50 and 100 m yr^{-1} over the subtropical gyre (Fig. 1b). There is a band of high subduction rates south of the Gulf Stream due to the lateral transfer; these kinematic calculations are broadly supported by Lagrangian diagnostics from a North Atlantic circulation model by Williams et al. (1995).

The gyre-scale subduction is associated with a buoyancy input into the mixed layer. Following a trajectory, a buoyancy input causes the mixed layer to lighten and shoal, which leads to mixed layer fluid being transferred into the stratified interior. MNW argued that this buoyancy input over the gyre scale is achieved through an atmospheric buoyancy input plus a wind-induced (Ekman) redistribution of buoyancy. However, this view of gyre-scale subduction may be modified by the rectified transport contribution by mesoscale eddies (Marshall 1997), which is particularly important in frontal zones and deep convection sites. In a region of eddy activity, the buoyancy budget following a time-mean trajectory can become misleading.[1]

Corresponding author address: Dr Richard G. Williams, Oceanography Laboratories, Department of Earth Sciences, University of Liverpool, Liverpool L69 7ZL, United Kingdom.
E-mail: ric@liv.ac.uk

[1] In regions of eddy activity, it is preferable to consider the area-averaged surface buoyancy loss over a density outcrop, which is related to a diapycnal volume flux and its convergence to a rate of water mass formation in density space (Walin 1982; Marshall 1997; Nurser et al. 1999). However, this water mass formation is *only* equivalent to the area-integrated subduction rate over a density outcrop in the limit of no diffusive mixing within the seasonal boundary layer (Marshall et al. 1999).

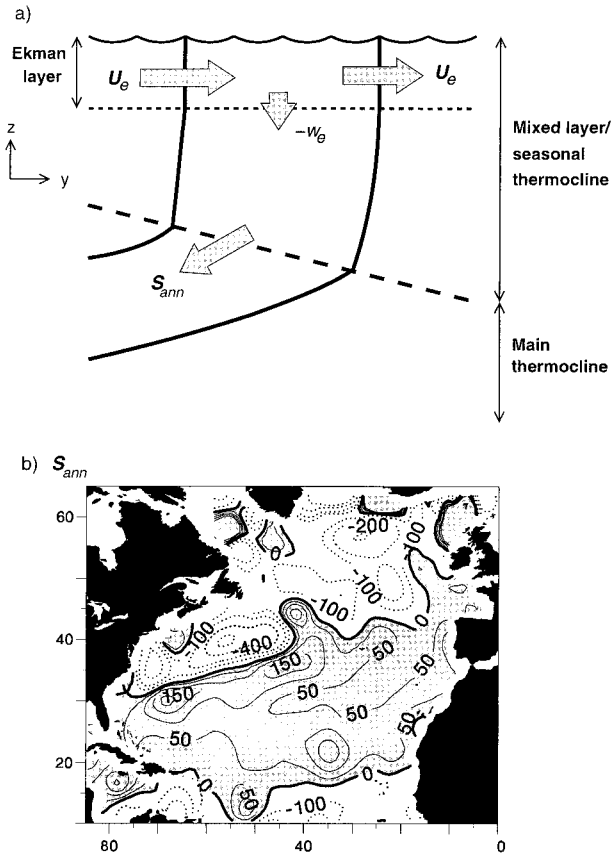

FIG. 1. (a) Schematic diagram of the subduction rate, S_{ann}, measuring the volume flux per unit horizontal area passing through a control surface into the main thermocline. The control surface is defined by the base of the end of winter mixed layer, H (long dashed line); $\mathbf{U}_e$ represents the horizontal Ekman volume flux and its convergence induces a vertical Ekman velocity, w_e. (b) Diagnostics of the subduction rate into the main thermocline (m yr^{-1}) (following the method described in MNW) where S_{ann} is evaluated in a Eulerian frame by the volume flux passing across the control surface, $S_{ann} = -w_H - \mathbf{u}_H \cdot \nabla H$, where w_H and $\mathbf{u}_H$ are climatological estimates of the vertical and horizontal velocities along the control surface. Shaded values denote subduction.

In this study, we extend the MNW analysis and consider how buoyancy is supplied to the surface ocean to drive gyre-scale subduction for climatological and interannual timescales. For convenience, we prefer to discuss the subduction process in terms of heat fluxes and temperature changes, although the data diagnostics are evaluated in terms of buoyancy fluxes. In section 2, the thermodynamics of subduction is briefly reviewed and connected with the heat content of a Lagrangian water column. In section 3, the thermodynamic budget associated with subduction is diagnosed over the North Atlantic from 1950 to 1992, and is analyzed in terms of the climatological average and interannual variability. In section 4, the implications of the study are discussed.

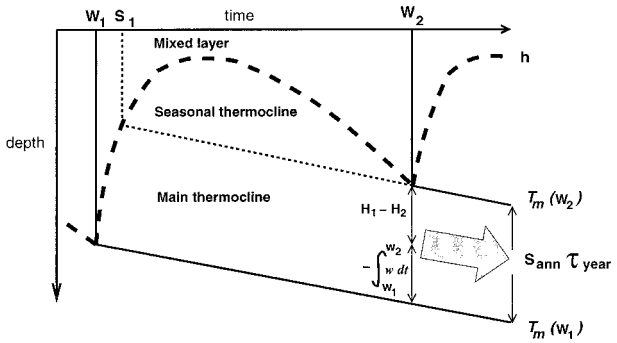

FIG. 2. Schematic diagram of a mixed-layer thickness cycle (thick dashed line) following a Lagrangian water column. The mixed layer is thick and cool at the end of the first winter, W_1, thins and warms over the spring and summer, then thickens and cools again until the end of the second winter, W_2. If there is an overall heat input into the column, the mixed layer becomes thinner and warmer over the annual cycle. This warming leads to fluid being subducted (during the subduction period from W_1 and S_1) and passing irreversibly into the main thermocline. In this Lagrangian frame, the subduction rate into the main thermocline, S_{ann}, consists of a vertical pumping contribution and a lateral transfer due to the shoaling of the winter mixed layer. Isotherms subducted from the end of winter mixed layer are depicted by the thin full lines. The base of the seasonal thermocline is marked by the thin dashed line.

2. Thermodynamics of subduction

The subduction process involves the seasonal cycle of the mixed layer, depicted in Fig. 2 following a Lagrangian water column. The mixed layer generally lightens and thins over spring and summer and becomes denser and thicker over autumn and winter, through the seasonal cycles in buoyancy forcing. Fluid is subducted into the

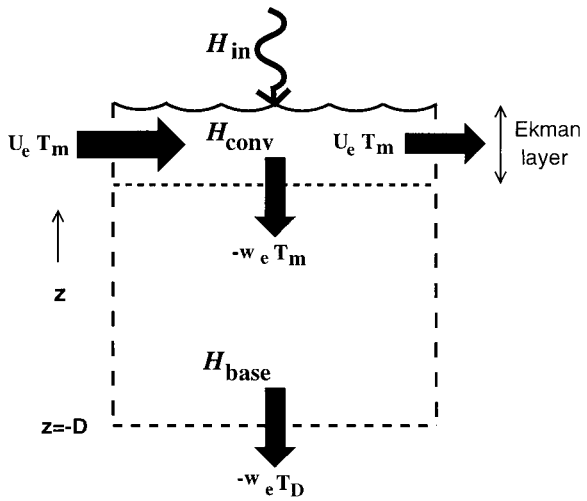

FIG. 3. Schematic diagram of the heat balance for a Lagrangian water column following the geostrophic flow. The water column increases its heat content through a surface heat flux, $\mathcal{H}_{in}$, plus the divergence of the horizontal Ekman heat flux, $\mathcal{H}_{conv} = -\rho_o C_w \nabla \cdot (\mathbf{U}_e T_m)$, and the heat flux pumped through the base of the water column, $\mathcal{H}_{base} = \rho_o C_w w_e T_D$; where U_e is the horizontal Ekman volume flux, $-w_e$ is the Ekman pumping, and T_m and T_D are the temperatures of the mixed layer and base of the water column.

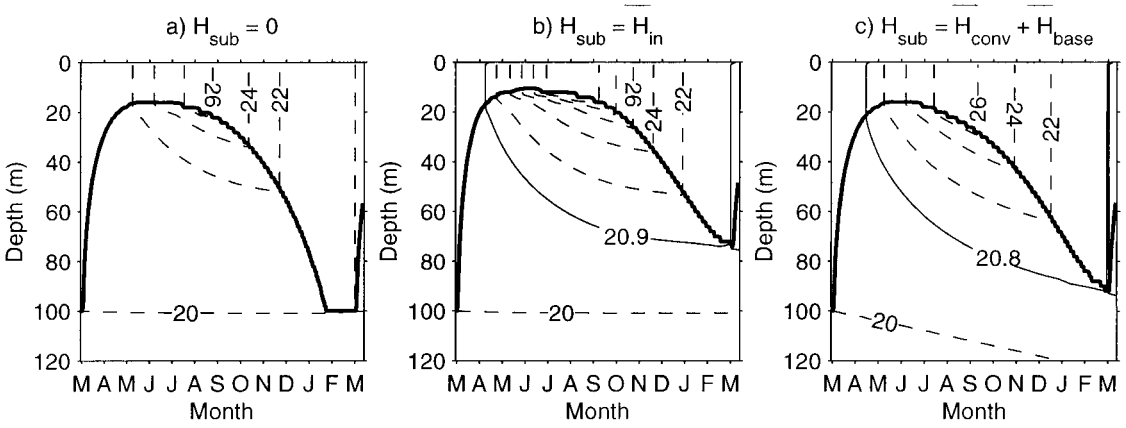

FIG. 4. Modeled annual cycle is mixed layer thickness (thick solid line) and temperature in the seasonal boundary layer (dashed lines): (a) no annual surface heat flux and no Ekman pumping; (b) annual surface heat flux of 10 W m^{-2} and no Ekman pumping; (c) no annual surface heat flux and an Ekman pumping of 25 m yr^{-1}. The isotherm marking the mixed layer temperature at the end of the second winter is denoted by a thin full line. In (a), when there is no surface annual heat input or Ekman pumping, there is no annual subduction. In (b), the annual surface heat flux leads to $\mathcal{H}_{sub}$ of 10 W m^{-2}, which increases the heat content and drives an annual subduction, S_{ann} of 28 m yr^{-1}, as revealed by the shoaling mixed layer. In (c), incorporating Ekman pumping and a seasonal mixed-layer temperature cycle of 10°C (without an annual surface heat flux) provides the same $\mathcal{H}_{sub}$ of 10 W m^{-2}. There is again an increase in heat content, a shoaling mixed layer, and an annual subduction, S_{ann}, of 33 m yr^{-1}.

thermocline during spring and summer and reentrained during autumn and winter. If there is an overall heat input, the mixed layer becomes lighter from one winter to the next winter, and a fraction of the subducted fluid becomes capped by the overlying mixed layer and passes into the main thermocline. Hence, the subduction process involves a thermal input into the mixed layer (Nurser and Marshall 1991). In this Lagrangian frame, the annual subduction rate into the main thermocline (Fig. 2) is given by (e.g., Williams et al. 1995)

$$S_{\text{ann}}\mathcal{T}_{\text{year}} = -\int_{W_1}^{W_2}\left(\frac{D_g h}{Dt} + w\right) dt$$

$$= H_1 - H_2 - \int_{W_1}^{W_2} w\, dt, \qquad (1)$$

where $D_g/Dt = \partial/\partial t + \mathbf{u}_g \cdot \boldsymbol{\nabla}$ is the Lagrangian rate of change following the geostrophic flow, $\mathbf{u}_g$ is the horizontal geostrophic velocity, w is the vertical velocity, h is the mixed layer thickness, H_1 and H_2 are the mixed layer thickness at the end of the first winter, W_1, and second winter, W_2, and $\mathcal{T}_{\text{year}}$ is 1 year. Note that when (1) is applied for a time-averaged flow, there may be an additional contribution from the rectified eddy transport (Marshall 1997).

MNW argued that the heat flux, $\mathcal{H}_{\text{sub}}$, driving gyre-scale subduction, is provided by the annual surface heat input, $\overline{\mathcal{H}}_{\text{in}}$, plus the annual convergence of the horizontal Ekman heat flux minus the heat pumped down through the base of the seasonal thermocline, which may be written as:[2]

$$\mathcal{H}_{\text{sub}} = \overline{\mathcal{H}}_{\text{in}} - \rho_o C_w \boldsymbol{\nabla} \cdot \overline{(\mathbf{U}_e T_m)} + \rho_o C_w \overline{w_e T_{\text{st}}}. \qquad (2)$$

Here, $\mathcal{H}_{\text{in}}$ is the surface heat flux, T_m and T_{st} are the temperatures of the mixed layer and the base of the seasonal thermocline, $\mathbf{U}_e$ is the horizontal Ekman volume flux, w_e is the vertical Ekman velocity (defined positive as upward), ρ_o is a reference density, and C_w is the specific heat capacity of water. The overline represents an annual average over the time $\mathcal{T}_{\text{year}}$ between the end of the first winter, W_1, to the second winter, W_2. The temperature at the base of the seasonal thermocline, $T_{\text{st}} = T_m$ during the subduction period defined between the end of winter W_1 and a later time S_1, and then $T_{\text{st}} = T_m(S_1)$ outside the subduction period from S_1 to the following end of winter W_2 (Fig. 2).

The heat flux driving subduction is closely related to the annual change in heat content following a Lagrangian column (derived in the appendix), which is given by

$$\mathcal{H}_{\text{sub}} \simeq \frac{\rho_o C_w}{\mathcal{T}_{\text{year}}}\left[\int_{-D}^{0} T\, dz\right]_{W_1}^{W_2} = \overline{\mathcal{H}}_{\text{in}} + \overline{\mathcal{H}}_{\text{conv}} + \overline{\mathcal{H}}_{\text{base}}, \qquad (3)$$

where the convergence of the Ekman heat flux is defined by

[2] MNW originally discussed the annual heat balance in terms of $\mathcal{H}_{\text{sub}} = \overline{\mathcal{H}}_{\text{in}} - \rho_o C_w[\overline{\mathbf{U}_e \cdot \boldsymbol{\nabla} T_m} + \overline{w_e(T_m - T_{\text{st}})}]$. We prefer the equivalent relation (2), since the terms have a clearer physical interpretation.

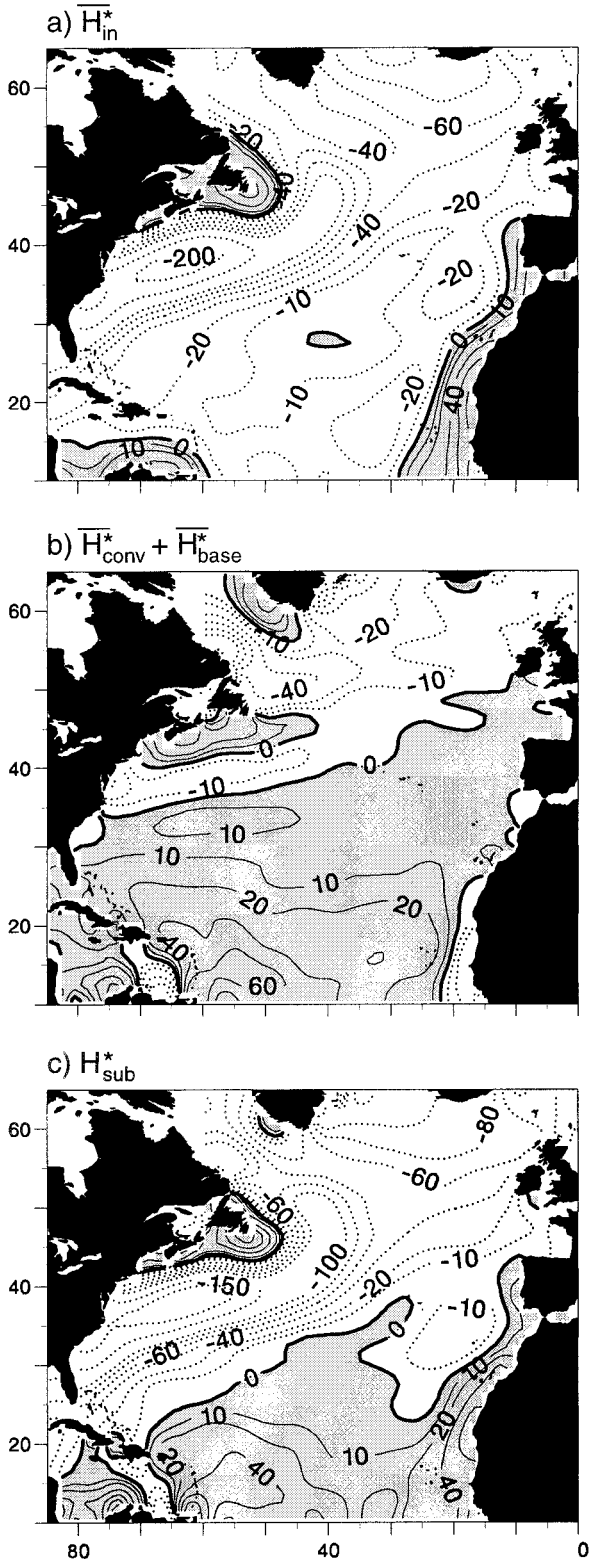

FIG. 5. Climatological average of the buoyancy flux, evaluated from 1950 to 1992, and converted to an effective heat flux (W m^{-2}): (a) surface buoyancy flux, $\overline{\mathcal{H}^*_{in}}$; (b) Ekman redistribution of buoyancy, $\overline{\mathcal{H}^*_{conv}} + \overline{\mathcal{H}^*_{base}}$; (c) buoyancy flux driving subduction, $\mathcal{H}^*_{sub}$. Shaded values represent a buoyancy input.

$$\mathcal{H}_{conv} \equiv -\rho_o C_w \nabla \cdot (\mathbf{U}_e T_m),$$

and the heat fluxed through the base of the column by

$$\mathcal{H}_{base} \equiv \rho_o C_w w_e T_D.$$

The heat content of the Lagrangian column following the geostrophic flow (Fig. 3) is altered by the annual surface heat input and convergence of the horizontal Ekman heat flux minus the heat pumped out through the base of the water column. Note that the combined value of $\mathcal{H}_{conv} + \mathcal{H}_{base} = -\rho_o C_w[\mathbf{U}_e \cdot \nabla T_m + w_e(T_m - T_D)]$ is not sensitive to the units used for measuring temperature. The heat flux driving subduction, $\mathcal{H}_{sub}$, in (2) is equivalent to (3) when the temperature at the base of the seasonal thermocline, T_{st}, is approximately the same as the temperature at the base of the Lagrangian column, T_D.

The thermodynamic relation (2) by MNW and our approximated version (3) is obtained after a number of simplifying assumptions: (i) the rectified volume flux and heat transfer by mesoscale eddies is neglected, (ii) entrainment during the subduction period is ignored, and (iii) heat advection by the geostrophic flow within the seasonal thermocline is neglected (following scaling in the appendix of MNW). Consequently, the MNW diagnostics are more relevant to the interior of the subtropical and subpolar gyres rather than boundary current regions on sites of deep convection. Despite these limitations, support for the MNW diagnostics is provided by coupled mixed layer and thermocline studies (Marshall and Marshall 1995) and general circulation model diagnostics of the subduction rate and heat balance for the ''Subduction Experiment'' in the North Atlantic (Spall et al. 2000).

The crucial implication of these thermodynamic relations (2) and (3) is that atmospheric forcing can affect subduction either directly through a surface influx of heat or indirectly by an Ekman redistribution of heat. These contrasting contributions are illustrated here with simplified mixed-layer model experiments in Fig. 4; following similar mixed layer studies by J. M. Frederiuk and J. F. Price (1985, unpublished manuscript) and Woods and Barkmann (1988). In these Lagrangian experiments, the winter mixed layer shoals and fluid is subducted into the thermocline *only* when there is an annual heat input. The heat input is provided here either from the annual surface heat flux (Fig. 4b) or the Ekman convergence of heat (Fig. 4c).

We next examine how $\mathcal{H}_{sub}$ and its contributions vary over climatological and interannual timescales over the North Atlantic.

3. Basin-scale diagnostics of the buoyancy flux driving subduction

a. Methodology

The thermodynamic balance for subduction (3) is extended to a buoyancy budget including freshwater fluxes and Ekman advection of density:

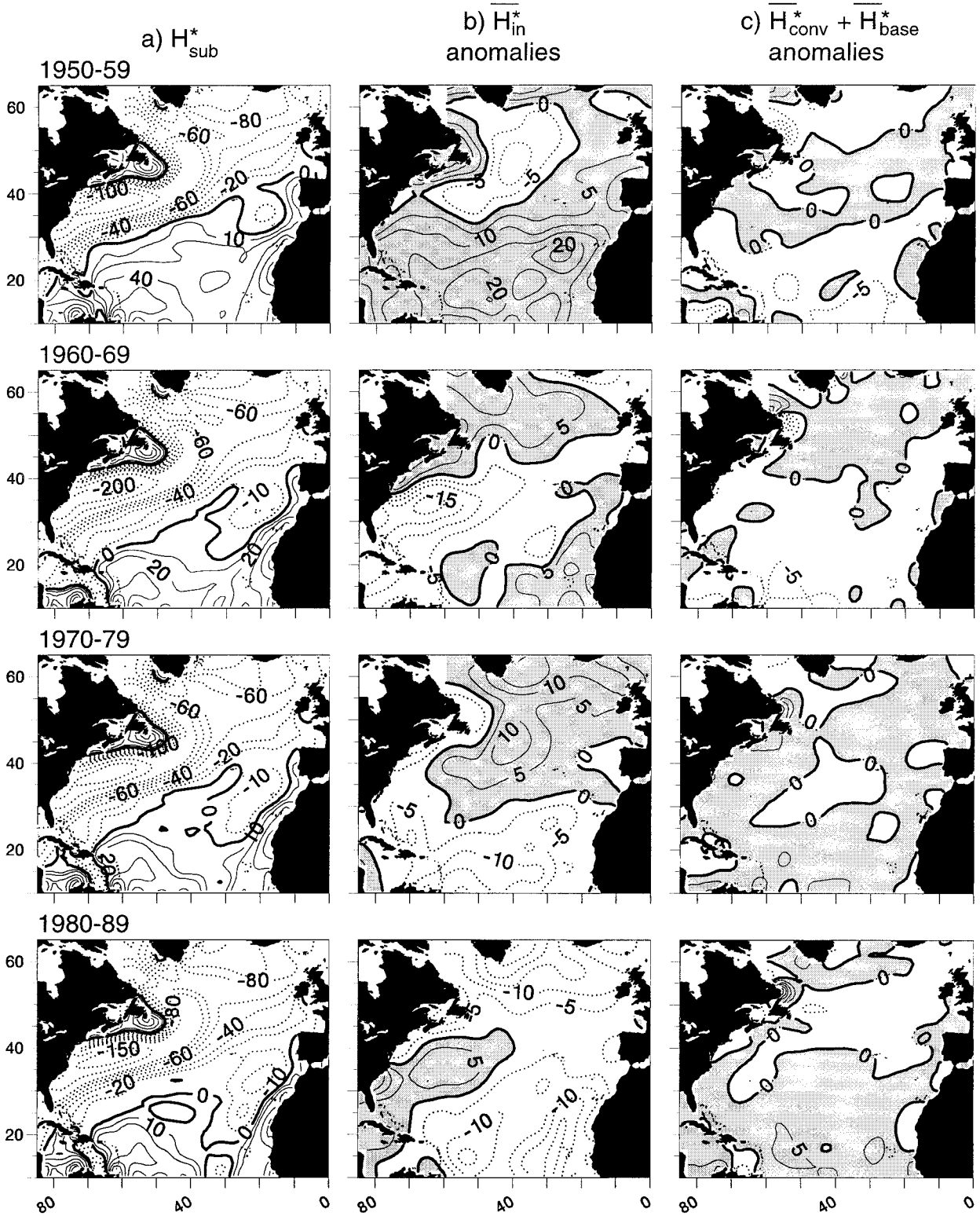

FIG. 6. Decadal maps of the effective buoyancy flux from 1950 to 1990 converted into an effective heat flux (W m^{-2}): (a) buoyancy-flux-driven subduction, $\mathcal{H}^*_{sub}$; (b) anomaly in surface buoyancy flux, $\Delta\overline{\mathcal{H}^*_{in}}$, relative to a climatological average from 1950 to 1992; (c) anomaly in Ekman redistribution of buoyancy, $\Delta\overline{\mathcal{H}^*_{conv}} + \Delta\overline{\mathcal{H}^*_{base}}$. The anomaly fields are shaded whenever the anomaly represents a buoyancy input.

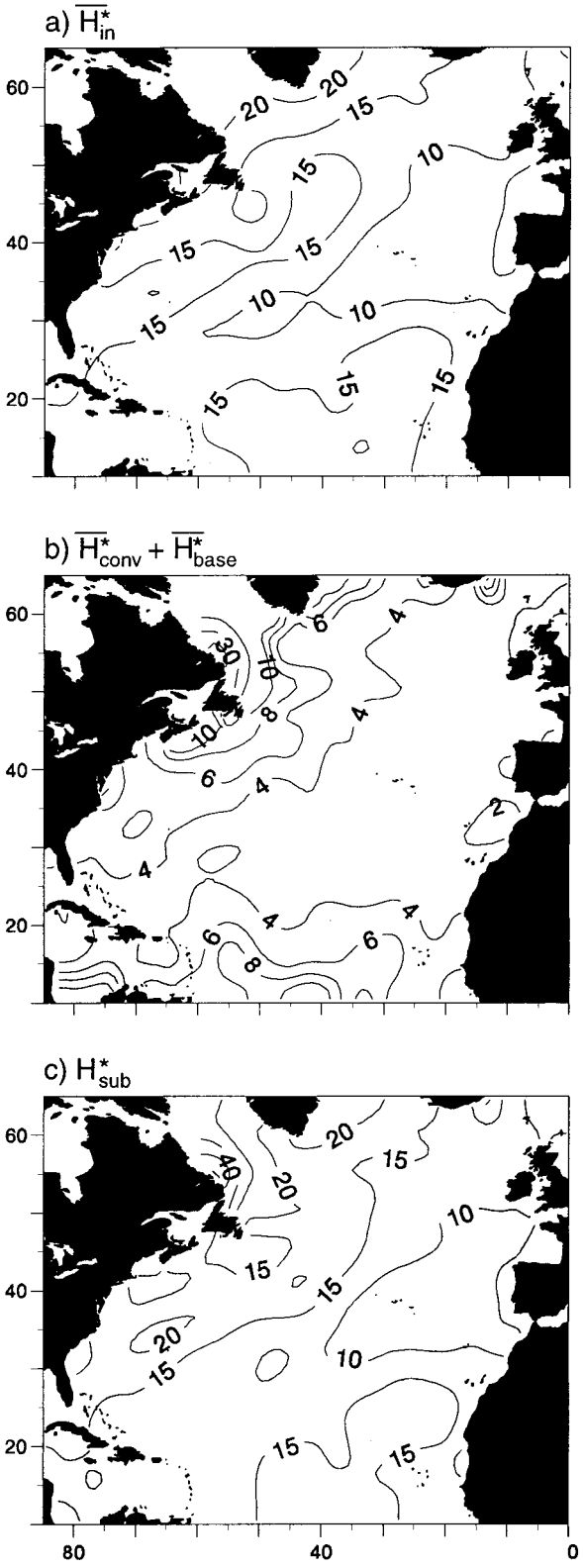

FIG. 7. Standard deviation in the buoyancy flux, evaluated from 1950 to 1992 and converted to an effective heat flux (W m^{-2}): (a) surface heat flux, $\overline{\mathcal{H}^*_{in}}$; (b) Ekman redistribution of buoyancy, $\overline{\mathcal{H}^*_{conv}} + \overline{\mathcal{H}^*_{base}}$; (c) buoyancy-flux-driven subduction, $\mathcal{H}^*_{sub}$.

$$\mathcal{B}_{sub} = \overline{\mathcal{B}}_{in} + \overline{\mathcal{B}}_{conv} + \overline{\mathcal{B}}_{base}, \quad (4)$$

where the surface buoyancy flux is $\mathcal{B}_{in} = (g\alpha/C_w)\,\mathcal{H}_{in} - g\beta\rho_o s_m(E - P)$, the convergence of the Ekman buoyancy flux is $\mathcal{B}_{conv} \equiv g\nabla\cdot(\mathbf{U}_e\rho_m)$, and the vertical buoyancy flux through the base of the column is $\mathcal{B}_{base} \equiv -gw_e\rho D$. Here α is the density expansion coefficient for temperature evaluated using the annual-mean mixed layer temperature, g is gravity, s_m is the salinity of the mixed layer, β is the haline contraction coefficient, E and P are the evaporation and precipitation rates, and ρ_m and ρ_D are the densities of the mixed layer and the base of the water column, respectively.

For convenience and following MNW, we prefer to discuss the contributions to the buoyancy budget (4) in terms of an effective heat flux, $\mathcal{H}^* \equiv C_w\mathcal{B}/(\alpha g)$, where the starred variable is a rescaled buoyancy flux.

The air–sea heat and freshwater fluxes, and wind stresses are taken from da Silva et al. (1994). The Ekman flux of buoyancy is then evaluated using monthly sea surface temperature (da Silva et al. 1994) and climatological monthly salinity (Levitus et al. 1994). The air–sea and Ekman buoyancy fluxes are evaluated every year from 1950 to 1992, where each year is defined as starting from the middle of March. For the buoyancy content changes, we choose to define the thickness of the column, D, by the thickness of the end of winter mixed layer, $h(W_1)$, and assume that $\rho_D = \rho(W_1)$.

We have developed a Lagrangian approach in order to understand the subduction process. When there is buoyancy input over a year, the winter mixed layer becomes lighter following a trajectory, which leads to more fluid being transferred into the main thermocline (Figs. 4b,c). Conversely, when there is buoyancy loss over a year, the winter mixed layer becomes denser following a trajectory, which leads to fluid being transferred from the main thermocline into the winter mixed layer/seasonal boundary layer. The horizontal scales that the surface and Ekman buoyancy fluxes vary over are generally much larger than the length of annual trajectories over the gyre interior. Consequently, for simplicity following MNW, we diagnose the buoyancy budget at fixed points, rather than take into account how the buoyancy fluxes change along a trajectory.

The buoyancy budget (4) is discussed first for the climatological balance and then for decadal and interannual variability.

b. Climatological buoyancy supply for subduction

The climatological-mean surface buoyancy flux is directed from the ocean into the atmosphere over much of the North Atlantic (Fig. 5a). The rescaled surface buoyancy flux, $\overline{\mathcal{H}^*_{in}}$, reaches more than -200 W m^{-2} over the Gulf Stream and reduces in magnitude to typically -10 W m^{-2} over the subtropical gyre; note that this buoyancy flux is dominated by the surface heat contribution rather than the freshwater contribution.

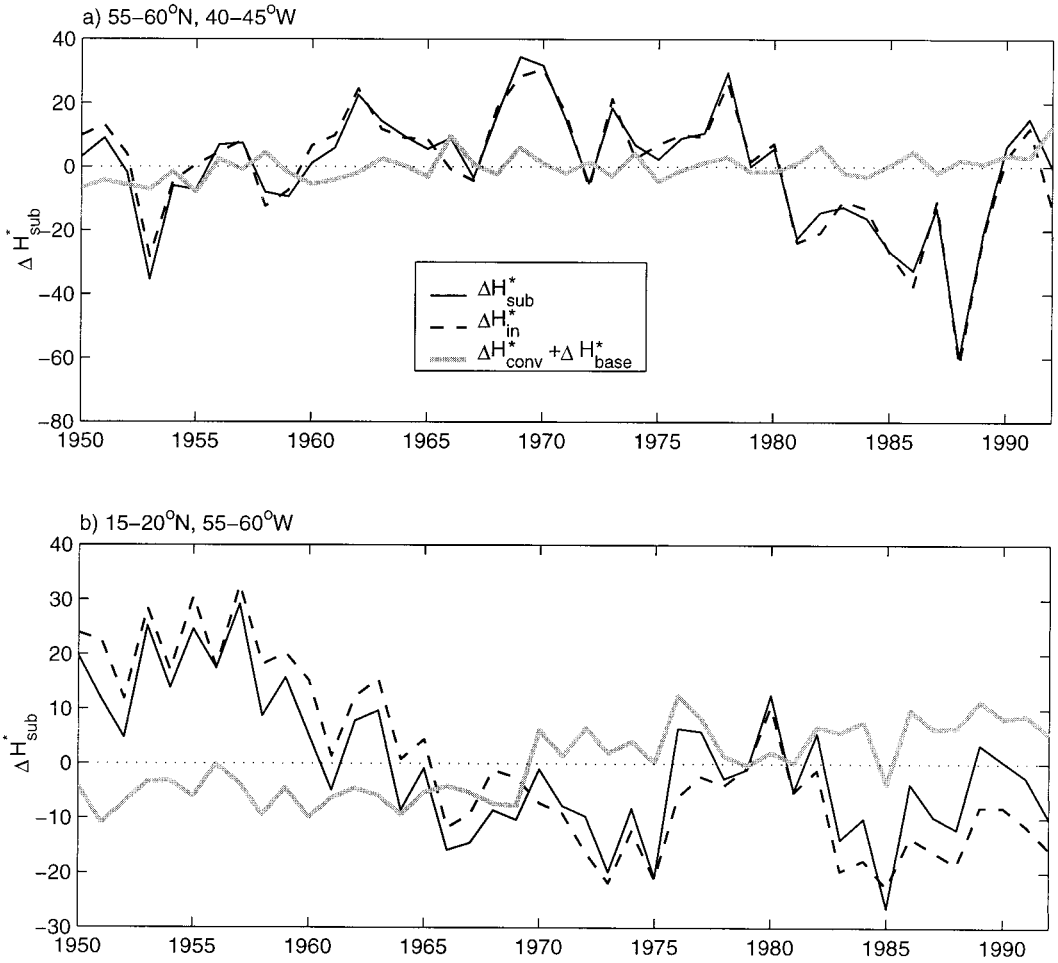

FIG. 8. Time series in the annual anomalies in buoyancy flux for subduction, $\Delta\mathcal{H}^*_{sub}$ (solid black line), surface buoyancy flux, $\Delta\overline{\mathcal{H}}^*_{in}$ (dashed line), and the Ekman redistribution of buoyancy, $\Delta\overline{\mathcal{H}}^*_{conv} + \Delta\overline{\mathcal{H}}^*_{base}$ (solid gray line), from 1950 to 1992 at two sites (W m^{-2}): (a) in the northwest Atlantic, 55°–60°N, 40°–45°W; (b) in the Tropics, 15°–20°N, 55°–60°W.

This buoyancy loss increases the density of the mixed layer and acts to transfer fluid from the thermocline into the mixed layer or seasonal boundary layer.

The Ekman redistribution of buoyancy, $\overline{\mathcal{H}}^*_{conv} + \overline{\mathcal{H}}^*_{base}$, provides a buoyancy input over much of the subtropical gyre and a buoyancy loss over the subpolar gyre, equivalent to a heat flux ranging typically from 10 to 20 W m^{-2} over the subtropical gyre (Fig. 5b).

The buoyancy input for subduction, $\mathcal{H}^*_{sub}$, is negative over much of the North Atlantic with positive values confined to the subtropical gyre and Tropics (Fig. 5c). The crucial result is that the buoyancy input driving gyre-scale subduction over the North Atlantic (as depicted in Fig. 1b) is provided by the Ekman redistribution of buoyancy (Fig. 5b) rather than the atmospheric input (Fig. 5a). These buoyancy diagnostics are broadly similar to those of MNW, even though they are evaluated annually from 1950 to 1992 rather than from climatological-mean data.

In principle, our estimate of $\mathcal{H}^*_{sub}$ should enable the annual subduction rate, S_{ann}, to be evaluated assuming a knowledge of the underlying stratification. However, we were unable to diagnose plausible maps for S_{ann} using this purely thermodynamic approach due to a combination of errors in the buoyancy budget and estimates of the underlying stratification.

c. *Decadal changes in buoyancy supply for subduction*

We now assess the extent to which the decadal and interannual variability in atmospheric forcing modifies the mechanisms by which buoyancy is supplied to drive subduction. Maps for the buoyancy flux supplied for subduction, $\mathcal{H}^*_{sub}$, averaged over each decade from 1950 to 1990 are shown in Fig. 6a. There is always the expected buoyancy loss at high latitudes and buoyancy gain at low latitudes. The zero line separating these regions generally runs from the southwest to the north-

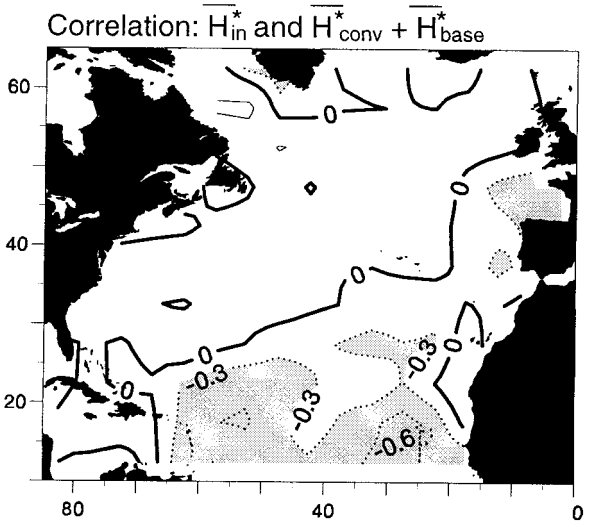

FIG. 9. Correlation map between the surface buoyancy flux, $\overline{\mathcal{H}^*_{in}}$, and the Ekman redistribution of buoyancy, $\overline{\mathcal{H}^*_{conv}} + \overline{\mathcal{H}^*_{base}}$. The correlation map is evaluated using the annual fields from 1950 to 1992. There is a generally negative correlation over the Tropics, which is statistically significant to a level of 95% where the correlation coefficient is greater than 0.3 in magnitude.

east across the North Atlantic. However, over the eastern Atlantic, there is a marked variability in the zero line, which varies from the most northern extent in the decade of 1950–59 and the most southern extent in the decade of 1980–89 (Fig. 6a).

The decadal anomalies in the surface buoyancy flux and the Ekman redistribution of buoyancy are shown in Figs. 6b and 6c with shading representing an anomalous buoyancy input; the anomaly is defined by the difference in the average over a decade and the average from 1950 to 1992. The interannual variations in $\mathcal{H}^*_{sub}$ are generally controlled by the anomalies in $\overline{\mathcal{H}}_{in}$, rather than $\overline{\mathcal{H}}_{conv} + \overline{\mathcal{H}}_{base}$. Over the Tropics, the anomalies in the surface and Ekman fluxes of buoyancy tend to oppose and partially compensate for each other (Figs. 6b,c).

d. Interannual changes in buoyancy supply for subduction

The standard deviation provides a measure of the interannual variability in the buoyancy supplied for subduction, evaluated from 1950 to 1992 (Fig. 7). The standard deviation in the surface buoyancy flux is equivalent to 15 W m^{-2} in terms of a heat flux. In contrast, the standard deviation of the Ekman redistribution of buoyancy is only equivalent to 4 W m^{-2} over much of the North Atlantic but rises to 20 W m^{-2} in the northwest Atlantic. Consequently, the resulting standard deviation in $\mathcal{H}^*_{sub}$ ranges from 10 to 20 W m^{-2}. Over the subtropical and tropical region, the interannual variability of $\mathcal{H}^*_{sub}$ is very large relative to its climatological value (Fig. 5c). The higher variability in $\mathcal{H}^*_{sub}$ over the Gulf Stream and subpolar gyre is less significant due to the larger magnitude of the climatological values there.

Time series of the anomalies of $\mathcal{H}^*_{sub}$ and its different buoyancy contributions (relative to their climatologies over 1950–92) are displayed for two locations in Fig. 8. Over the northwest Atlantic (55°–60°N, 40°–45°W), the climatological $\mathcal{H}^*_{sub}$ is -50 W m^{-2} and is controlled by the surface buoyancy flux. The interannual variability of $\mathcal{H}^*_{sub}$ in this region is likewise strongly controlled by the variability in the surface buoyancy flux rather than the Ekman contribution (Fig. 8a). In the Tropics (15°–20°N, 55°–60°W), the climatological $\mathcal{H}^*_{sub}$ is -41 W m^{-2} and is, instead, controlled by the Ekman redistribution of buoyancy. However, the interannual variability of $\mathcal{H}^*_{sub}$ is again largely controlled by the variability in the surface buoyancy flux (Fig. 8b). The variability in $\mathcal{H}^*_{sub}$ is smaller than that for $\mathcal{H}^*_{in}$ due to a partial compensation between $\mathcal{H}^*_{in}$ and $\mathcal{H}^*_{conv} + \mathcal{H}^*_{base}$ (Fig. 8b).

This partial compensation is revealed in a map of correlation coefficients between $\mathcal{H}^*_{in}$ and $\mathcal{H}^*_{conv} + \mathcal{H}^*_{base}$ (Fig. 9). The surface buoyancy flux and Ekman redistribution are not significantly correlated over most of the North Atlantic. There is though a significant negative correlation over the Tropics and southern subtropical gyre (shaded values being significant to a level of 95%). The compensation between the surface and Ekman buoyancy fluxes is due to the variability in the latent and incoming solar heat fluxes correlating with the variability in the Ekman flux. The related variability in the Ekman flux is due to the variability in wind stress rather than sea surface temperature. Consequently, the likely controlling mechanism is that an increase in wind stress increases the northward Ekman flux of buoyancy, as well as reducing the surface buoyancy gain through enhanced evaporation.

Given the significant interannual variation in $\overline{\mathcal{H}}_{in}$, we now examine whether the implied subduction ever ceases for a particular year through an overall heat loss leading to a widespread thickening of the winter mixed layer. A time series of the integrated area over which $\mathcal{H}^*_{sub}$ is positive is shown in Fig. 10a. There are significant decadal and interannual variations with the greatest area over which there is a buoyancy input occurring in the 1950s and a minimum area occurring in 1962, 1984, and 1985. However, there are always some regions over which there is a buoyancy input and, hence, implied gyre-scale subduction. The most extensive area over which there is a buoyancy input for subduction occurs in 1950, whereas the most limited buoyancy input occurs in 1985 (Figs. 10b,c).

e. Connection with the North Atlantic Oscillation

The dominant mode of atmospheric variability over the North Atlantic is associated with the North Atlantic Oscillation (NAO) (Hurrell 1995), which alters air–sea fluxes (Cayan 1992a) and the patterns of winter con-

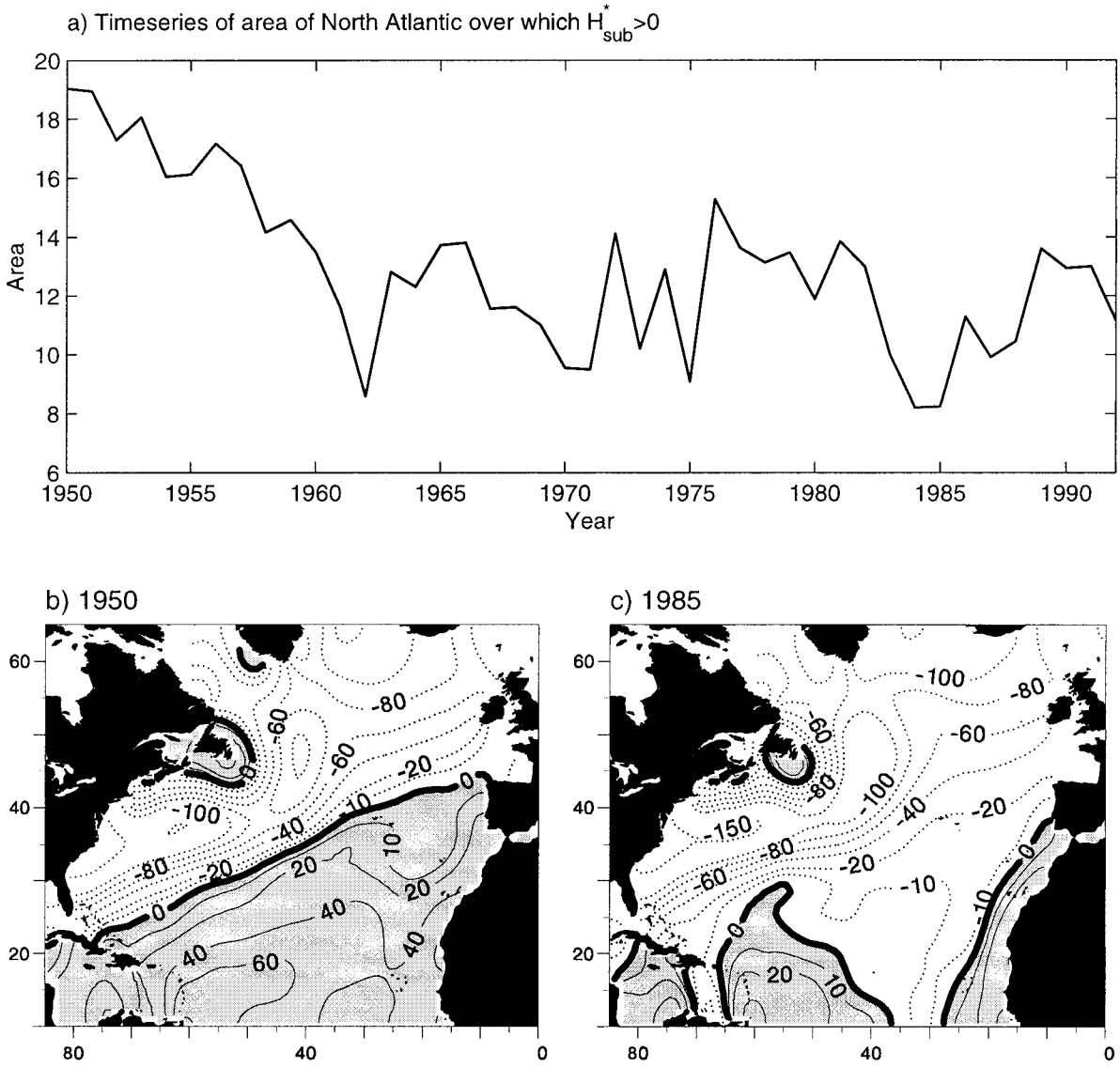

FIG. 10. (a) Time series for the area (10^{12} m^2) over which $\mathcal{H}^*_{sub}$ is positive over the domain from 1950 to 1992. Maps of $\mathcal{H}^*_{sub}$ are shown for two limiting cases (W m^{-2}): (b) 1950 and (c) 1985; shaded values represent a buoyancy input. Note the poleward extent of the zero line in 1950 and the equatorward extent in 1985.

vection (Dickson et al. 1996; Williams et al. 2000). There is a tripole pattern in the correlation between the wintertime surface heat flux and the NAO (Fig. 11a), which is due to the wintertime patterns of the sensible and latent heat flux (Cayan 1992a). For example, this pattern is evident in the decadal maps for surface heat flux in Fig. 6b, which shows a characteristic NAO$_-$ state for 1960–69 and a NAO$_+$ state in 1980–89.

The correlation pattern between $\mathcal{H}^*_{sub}$ and the NAO (Fig. 11b) is broadly similar to that between the winter heat flux and the NAO (Fig. 11a). There is a negative correlation over the subpolar gyre with values less than -0.3 and a positive correlation over the Gulf Stream region with values greater than 0.5; note that a correlation of 0.3 is statistically significant to a level of 95%. Hence, over the Gulf Stream, increased heat loss during a NAO$_-$ state leads to $\mathcal{H}^*_{sub}$ becoming more negative, which implies a greater transfer or induction of thermocline fluid into the mixed layer.

The similarity in the correlation maps in Fig. 11 is due to the variability in the air–sea heat flux dominating the variability in $\mathcal{H}^*_{sub}$. The only significant differences in these correlation maps are over the Tropics: for $\mathcal{H}^*_{sub}$,there is a smaller region with a significant negative correlation to the NAO, while for the winter surface heat flux there is a larger region with a negative correlation to the NAO. The reduced area of negative correlation for $\mathcal{H}^*_{sub}$ is due to $\overline{\mathcal{H}}_{conv} + \overline{\mathcal{H}}_{base}$ in the Tropics

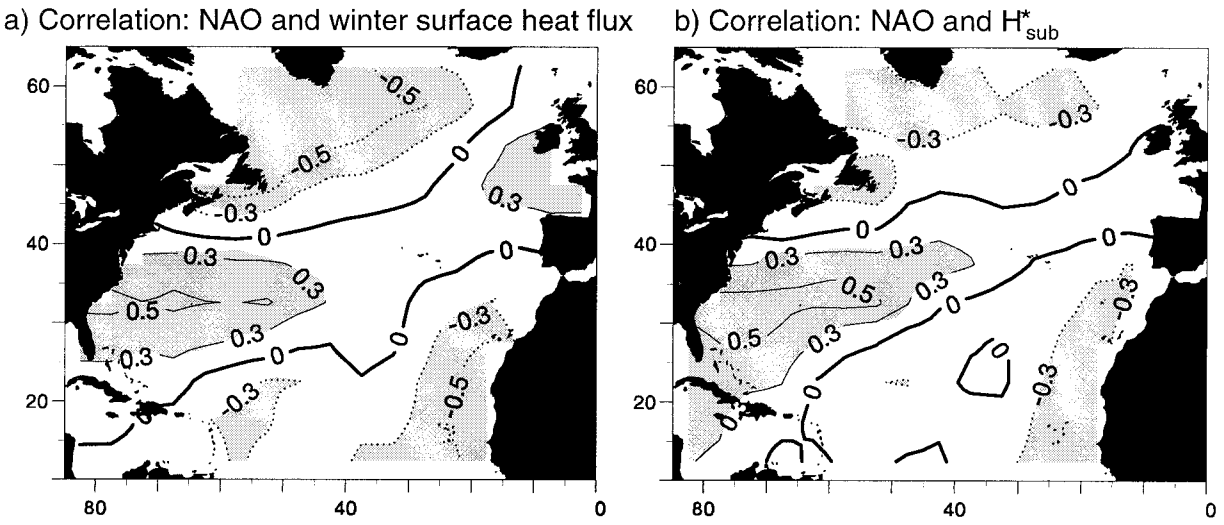

FIG. 11. Correlation map between the North Atlantic Oscillation index (Hurrell 1995) and (a) the winter surface heat flux and (b) $\mathcal{H}^*_{sub}$. The correlation maps are evaluated every year from 1950 to 1992. Statistically significant values at a level of 95% have a correlation coefficient greater than 0.3 in magnitude.

being positively correlated with the NAO (with a highest value being 0.61), which partially compensates for the negative correlation between $\overline{\mathcal{H}}_{in}$ and the NAO.

4. Discussion

The subduction process provides a mechanism by which atmospheric forcing alters the heat content and water mass structure of the upper ocean. Subduction is achieved over the gyre scale through a combination of a surface buoyancy input from the atmosphere and an Ekman redistribution of buoyancy from the Tropics.

The buoyancy flux, $\mathcal{H}^*_{sub}$, driving gyre-scale subduction is analyzed here using time series of surface and Ekman buoyancy fluxes from 1950 to 1992 over the North Atlantic. There are significant errors in our buoyancy diagnostics due to the errors in the surface heat flux, which are at least ± 25 W m^{-2}. Our general conclusions remain unaltered, even when repeating the thermodynamic analysis with National Centers for Environmental Prediction reanalysis data (Kalnay et al. 1996), although the detailed pattern for $\mathcal{H}^*_{sub}$ does alter for any particular year. Our gyre-scale study does not take into account the rectified contribution of eddies (Marshall 1997), which becomes important along frontal zones and deep convections sites.

Our climatological analysis over the North Atlantic suggests that gyre-scale subduction is not achieved by an atmospheric input of buoyancy, but rather by an Ekman redistribution of buoyancy. MNW obtain the same result using a similar thermodynamic approach, but with different climatological data. In addition, Spall et al. (2000) diagnose that the same balance operated over the ''Subduction Experiment'' in the North Atlantic.

The dominant contributions to the buoyancy budget for gyre-scale subduction vary for interannual timescales. The variations in the buoyancy supplied for subduction are instead controlled by the changes in the surface buoyancy flux rather than the changes in the Ekman buoyancy flux. Consequently, $\mathcal{H}^*_{sub}$ has a tripole pattern in its correlation with the North Atlantic Oscillation. For example, over the Gulf Stream, there is enhanced convection during a NAO_- state and reduced convection during a NAO_+ state, as highlighted by Dickson et al. (1996). Accordingly, over the Gulf Steam, there should be an enhanced or reduced transfer/induction of thermocline fluid into the mixed layer during NAO_- and NAO_+ states, respectively.

The interannual variations in the buoyancy flux driving subduction are particularly large compared with its climatological value over the Tropics and much of the subtropical gyre. Over the eastern half of the subtropical gyre $\mathcal{H}^*_{sub}$ often changes sign for different years, suggesting that fluid can either be subducted from or inducted into the mixed layer here. The variability in $\mathcal{H}^*_{sub}$ is weaker than expected over the Tropics due to a partial compensation between the surface and Ekman buoyancy fluxes. This compensation is due to an increase in the wind reducing the surface buoyancy input, while also increasing the poleward Ekman buoyancy flux. Hence, the variability in gyre-scale subduction should be greater over the subpolar gyre and northern flank of the subtropical gyre, rather than over the Tropics and southern flank of the subtropical gyre.

Acknowledgments. This study was supported by the UK NERC COAPEC programme (NER/T/S/2000/00305). We thank David Marshall for helpful discussions, and AM is grateful to Plymouth Marine Laboratory for providing host facilities.

APPENDIX

Lagrangian Annual Heat Budget

In order to obtain more physical insight into how heat transfers modify subduction, we examine the change in heat content following a Lagrangian column (Fig. 2). The heat equation integrated over a column of thickness D extending from the surface to the base of the winter mixed layer is given by

$$\int_{-D}^{0} \left(\frac{D_g T}{Dt} + w \frac{\partial T}{\partial z} \right) dz + \mathbf{U}_e \cdot \boldsymbol{\nabla} T_m = \frac{\mathcal{H}_{\text{in}}}{\rho_o C_w}, \quad \text{(A1)}$$

where entrainment and diabatic fluxes at the base of the winter mixed layer and rectified eddy contributions are neglected. Here, $D_g/Dt = \partial/\partial t + \mathbf{u}_g \cdot \boldsymbol{\nabla}$ is the Lagrangian rate of change following the geostrophic velocity, $\mathbf{u}_g$, w is the vertical velocity, and $\mathbf{U}_e \cdot \boldsymbol{\nabla} T_m$ is the Ekman advection of temperature over the water column (with the Ekman layer assumed to be within the mixed layer).

Assuming that the vertical velocity is approximately constant with depth below the Ekman layer, with a value $w(z) \sim w_e$, then the Lagrangian change in heat content following the geostrophic flow is given from (A1) by

$$\int_{-D}^{0} \frac{D_g T}{Dt} dz = \frac{\mathcal{H}_{\text{in}}}{\rho_o C_w} - \mathbf{U}_e \cdot \boldsymbol{\nabla} T_m - w_e (T_m - T_D), \quad \text{(A2)}$$

where T_D is the temperature at the base of the water column, $z = -D$. This balance (A2) is physically easier to interpret by combining the Ekman terms,

$$\boldsymbol{\nabla} \cdot (\mathbf{U}_e T_m) = \mathbf{U}_e \cdot \boldsymbol{\nabla} T_m + w_e T_m,$$

where $w_e \equiv \boldsymbol{\nabla} \cdot \mathbf{U}_e$, to give

$$\int_{-D}^{0} \frac{D_g T}{Dt} dz = \frac{\mathcal{H}_{\text{in}}}{\rho_o C_w} - \boldsymbol{\nabla} \cdot (\mathbf{U}_e T_m) + w_e T_D. \quad \text{(A3)}$$

Integrating (A3) over an annual cycle, from the end of the first winter W_1 to the second winter W_2, gives

$$\frac{\rho_o C_w}{\mathcal{T}_{\text{year}}} \left[\int_{-D}^{0} T \, dz \right]_{W_1}^{W_2} = \overline{\mathcal{H}}_{\text{in}} - \rho_o C_w \boldsymbol{\nabla} \cdot \overline{(\mathbf{U}_e T_m)} + \rho_o C_w \overline{w_e T_D}. \quad \text{(A4)}$$

Hence, the annual change in heat content of the water column is driven by the surface heat flux, the convergence of the Ekman heat flux, and the heat pumped out of the base of the column. This change in heat content does not account for the heat advected by the baroclinic velocity shear within the seasonal thermocline since this contribution is relatively small (see appendix of MNW). The annual change in heat content (A4) is approximately equivalent to the heat flux driving subduction, $\mathcal{H}_{\text{sub}}$, in (2) when the temperature at the base of the winter mixed layer, T_D, is approximately the same as that at the base of the seasonal thermocline, T_{st}.

REFERENCES

Bjerknes, J., 1964: Atlantic air–sea interaction. *Advances in Geophysics*, Vol. 20, Academic Press, 1–82.

Cayan, D. R., 1992a: Latent and sensible heat flux anomalies over the northern oceans: The connection to monthly atmospheric circulation. *J. Climate,* **5,** 354–369.

——, 1992b: Latent and sensible heat flux anomalies over the northern oceans: Driving the sea surface temperature. *J. Phys. Oceanogr.,* **22,** 859–881.

da Silva, A. M., C. C. Young, and S. Levitus, 1994: *Atlas of Surface Marine Data 1994.* Vol. 1: *Algorithms and Procedures,* NOAA Atlas NESDIS 6, 83 pp.

Dickson, R., J. Lazier, J. Meinke, P. Rhines, and J. Swift, 1996: Long term coordinated changes in the convective activity of the North Atlantic. *Progress in Oceanography,* Vol. 38, Pergamon, 241–295.

Hurrell, J. W., 1995: Decadal trends in the North Atlantic Oscillation: Regional temperatures and precipitation. *Science,* **269,** 676–679.

Kalnay, E., and Coauthors, 1996: The NCEP/NCAR 40-Year Reanalysis Project. *Bull. Amer. Meteor. Soc.,* **77,** 437–471.

Kushnir, Y., 1994: Interdecadal variations in North Atlantic sea surface temperature and associated atmospheric conditions. *J. Climate,* **7,** 141–157.

Levitus, S., R. Burgett, and T. P. Boyer, 1994: *World Ocean Atlas 1994.* Vol. 3: *Salinity,* NOAA Atlas NESDIS 3, 99 pp.

Marshall, D., 1997: Subduction of water masses in an eddying ocean. *J. Mar. Res.,* **55,** 201–222.

——, and J. C. Marshall, 1995: On the thermodynamics of subduction. *J. Phys. Oceanogr.,* **25,** 138–151.

Marshall, J. C., A. J. G. Nurser, and R. G. Williams, 1993: Inferring the subduction rate and period over the North Atlantic. *J. Phys. Oceanogr.,* **23,** 1315–1329.

——, D. Jamous, and J. Nilsson, 1999: Reconciling thermodynamic and dynamic methods of computing water-mass transformation rates. *Deep-Sea Res.,* **46,** 545–572.

Nurser, A. J. G., and J. C. Marshall, 1991: On the relationship between subduction rates and diabatic forcing of the mixed layer. *J. Phys. Oceanogr.,* **21,** 1793–1802.

——, R. Marsh, and R. G. Williams, 1999: Diagnosing water mass formation from air–sea fluxes and surface mixing. *J. Phys. Oceanogr.,* **29,** 1468–1487.

Spall, M. A., R. A. Weller, and P. W. Furey, 2000: Modelling the three-dimensional upper ocean heat budget and subduction rate during the Subduction Experiment. *J. Geophys. Res.,* **105,** 26 151–26 166.

Walin, G., 1982: On the relation between sea-surface heat flow and thermal circulation in the ocean. *Tellus,* **34,** 187–195.

Williams, R. G., M. A. Spall, and J. C. Marshall, 1995: Does Stommel's mixed layer ''demon'' work? *J. Phys. Oceanogr.,* **25,** 3089–3102.

——, A. J. McLaren, and M. J. Follows, 2000: Estimating the convective supply of nitrate and implied variability in export production over the North Atlantic. *Global Biogeochem. Cycles,* **14,** 1299–1313.

Woods, J. D., and W. Barkmann, 1988: A Lagrangian mixed-layer model of Atlantic 18°C water formation. *Nature,* **319,** 574–576.